ISBN: 978-3-95450-202-8 doi:10.18429/JACoW-HB2018-TUP2WE03

RADIATION DAMAGE CALCULATION IN PHITS AND BENCHMARKING EXPERIMENT FOR CRYOGENIC-SAMPLE HIGH-ENERGY PROTON IRRADIATION

Y. Iwamoto*, H. Matsuda, S. Meigo, D. Satoh,
Japan Atomic Energy Agency, Tokai, Ibaraki 319-1195, Japan
T. Nakamoto, M. Yoshida, KEK, Tsukuba, Ibaraki 305-0801, Japan
Y. Ishi, Y. Kuriyama, T. Uesugi, H. Yashima, T. Yoshiie,
KURNS, Kyoto University, Kumatori, Osaka 590-0494, Japan
T. Shima, RCNP, Osaka University, Ibaraki, Osaka 567-0047, Japan
R. M. Ronningen, FRIB, Michigan State University, East Lansing, MI 48824, USA
K. Niita,
Research Organization for Information Science and Technology, Tokai, Ibaraki 319-1106, Japan

Abstract

The radiation damage calculation model in the Particle and Heavy Ion Transport code System (PHITS) has been developed to calculate the displacement per atom (DPA) value due to the target Primary Knock-on Atom (PKA) created by the projectile and the secondary particles which include all particles created from the sequential nuclear reactions. For the DPA value in the high-energy (E>100 MeV) proton incident reactions, a target PKA created by the secondary particles was more dominant than a target PKA created by the projectile. To validate prediction of displacement cross sections in copper and aluminum irradiated by >100 MeV protons, we developed a proton irradiation device with a Gifford-McMahon (GM) cryocooler to cryogenically cool wire samples. By using this device, the defect-induced electrical resistivity changes related to the displacement cross section of copper were measured under irradiation with 125, 200 MeV and 3 GeV protons and that of aluminum under 200 MeV protons at cryogenic temperature. A comparison of the experimental displacement cross sections with the calculated results indicates that the athermal recombination-corrected displacement cross section (arc-dpa) provides better quantitative descriptions than the conventional displacement cross section (NRT-dpa) used widely for radiation damage estimation.

INTRODUCTION

As the power of proton and heavy-ion accelerators increases, the prediction of the structural damage to materials under irradiation is essential. Radiation damage of materials is usually measured as a function of the average number of displaced atoms per all atoms in a material. DPA is related to the number of Frenkel pairs, where a Frenkel pair is defined as a vacancy and a self-interstitial atom in the irradiated material. For example, ten DPA means each atom in the material has been displaced from its lattice site of the material an average of ten times. DPA serves as a quantitative measure of damage: DPA=$\sigma_d\phi$. σ_d is the displacement cross section; and ϕ is the irradiation fluence. The level of the radiation damage in DPA units is used, for example, to estimate radiation damage of those materials experiencing significant irradiation by primary and "secondary particles" which include all particles created from the sequential nuclear reactions at high-energy (E>100 MeV), high intensity facilities such as the Facility for Rare Isotope Beams (FRIB) [1], the Japan Proton Accelerator Research Complex (J-PARC) [2], European Spallation Source (ESS) [3], and others. The DPA value is a useful measure in correlating results determined by different particles and fluxes in an irradiation environment. It is however difficult to measure the DPA value in high energy reactions and the relationships between DPA and material property changes are at present unclear.

SRIM [4] is one of the major codes used to estimate radiation damage in the low-energy reaction region. SRIM treats the transport of the projectile with its Coulomb scattering and makes an approximation of cascade damage. As SRIM does not treat nuclear reactions, the calculated damage is that produced by the primary knock-on atom, PKA, because damage created by the "secondary particles" produced in nuclear reactions is not considered. On the other hands, the nuclear reaction models in advanced Monte Carlo particle transport code systems such as PHITS [5], MARS15 [6], FLUKA [7] and MCNPX [8] have been developed for the calculation of the transport of particles, nuclear reactions between particles and materials, energy distribution of PKAs, and DPA values [9, 10].

For validation of calculated DPA values, one possibility is to measure displacement cross-sections in relation to changes in electrical resistivity at cryogenic temperature. The number of surviving defects is related experimentally to defect-induced changes in the electrical resistivity of metals at around 4 K, where the recombination of Frenkel pairs by thermal motion is well suppressed. The increase in electrical resistivity due to incident high-energy protons can be used to determine the experimental displacement cross section. Recently, we developed a proton irradiation device with a Gifford-McMahon (GM) cryocooler to cryogenically cool wire samples. By using this device, we measured

* iwamoto.yosuke@jaea.go.jp

ISBN: 978-3-95450-202-8 doi:10.18429/JACoW-HB2018-TUP2WE03

the defect-induced electrical resistivity changes related to the displacement cross section of copper were measured under irradiation with 125 MeV [11], 200 MeV [12] and 3 GeV [13, 14] protons and that of aluminum under irradiation with 200 MeV [12] protons at cryogenic temperature.

RADIATION DAMAGE MODEL IN PHITS

High-energy ions traveling through a target lose their energy in three ways: nuclear reactions, electron excitations, and Coulomb scattering. The lower the projectile energy, the higher is the energy transfer to the target atom via Coulomb scattering. The target atom directly hit by the projectile usually has much lower energy than the projectile itself and, therefore, has a larger cross-section for Coulomb scattering with other target atoms. Thus, the target PKA creates localized cascade damage where many target atoms are displaced from their original lattice site, leav-ing the same number of interstitials and vacancies. These point defects and their clusters affect the macroscopic material properties, such as hardness [15].

The conditions of various irradiations will be described by using the damage energy to characterize the displacement cascade. This is defined as the initial energy of target PKA, corrected for the energy lost to electronic excitations by all of the particles composing the cascade. There are mainly two ways to produce the target PKA. One is the Coulomb scattering due to PKA's directly created by the projectile, and the other is that due to PKA's created by the secondary particles. For the secondary particle production, the conservation of energy and momentum is sustained in each event using nuclear reactions for high energy particles.

To estimate the displacement cross sections, the "NRT" formalism of Norgett, Robinson, and Torrens [16] is employed as a standard to determine the fraction of the energy of the target PKA to produce damage, e.g., further nuclear displacements. The displacement cross sections can be evaluated using the following expression:

$$\sigma_{NRT} = \int_{t_d}^{t_{max}} d\sigma_{sc}/dt \cdot N_{NRT} dt \tag{1}$$

where $d\sigma_{sc}/dt$ is a universal one-parameter differential scattering cross section equation using the screening functions $f(t^{1/2})$ in reduced notation is expressed as:

$$d\sigma_{sc}/dt = \pi a_{TF}^2/2 \cdot f(t^{1/2})/t^{3/2} \tag{2}$$

where a_{TF} is the screening distance and t is a dimensionless collision parameter defined by

$$t \equiv \epsilon^2 T/T_{max} = \epsilon^2 \sin^2(\theta/2) \tag{3}$$

where θ is the center-of-mass (CM) scattering angle. One-parameter "t" in a function is convenient to integrate Eq. (1) in the PHITS calculation. T is the transferred energy to the target, and T_{max} is the maximum transferred energy as

$$T_{max} = 4M_1M_2/(M_1 + M_2)^2 \cdot E_p \tag{4}$$

where E_p is the projectile or secondary energy. ϵ is the dimensionless energy as

$$\epsilon = a_{TF}E/(Z_1Z_2e^2) \tag{5}$$

$f(t^{1/2})$ in Eq. (2) can be generalized to provide a one parameter universal differential scattering cross section equation for interatomic potentials such as screened and unscreened Coulomb potentials. The general form is

$$f(t^{1/2}) = \lambda t^{1/2-m}[1 + (2\lambda t^{1-m})^q]^{-1/q} \tag{6}$$

where λ, m, and q are fitting variables, with λ=1.309, m=1/3 and q=2/3 [9] for the Thomas-Fermi version of $f(t^{1/2})$.

N_{NRT} in Eq. (1) is the number of defects produced in irradiated material as shown in the following equation:

$$N_{NRT} = (0.8 \cdot T_d)/(2 \cdot E_d) \tag{7}$$

The displacement threshold energy E_d is typically in the range between 10 and 90 eV for most metals [9]. The damage energy, T_d, is the energy transferred to the lattice atoms and is reduced by the losses from electronic stopping in the atom displacement cascade and is given:

$$T_d = T/(1 + k_{cascade} \cdot g(\epsilon)) \tag{8}$$

where T is the transferred energy to target atom given by Eq. (3) as

$$T = T_{max} \cdot t/\epsilon_p^2 \tag{9}$$

where ϵ_p is the dimensionless projectile energy given by Eq. (4) and the projectile energy E_p. The parameters $k_{cascade}$, and g(ϵ) are as follows:

$$k_{cascade} = 0.1337Z_2^{1/6}(Z_2/A_2)^{1/2} \tag{10}$$

$$g(\epsilon) = \epsilon + 0.40244 \cdot \epsilon^{3/4} + 3.4008 \cdot \epsilon^{1/6} \tag{11}$$

The dimensionless transferred energy, ϵ, is given by Eqs. (5) and (7).

In Eq. (1), t_{max}, which is dimensionless, is equal to ϵ^2 from Eq. (3) when $\theta = \pi$. t_d is the displacement threshold energy, also dimensionless, given by Eq. (5).

DPA Distributions in Thick Targets

Based on the above formalism, we calculated DPA distributions in thick copper and tungsten targets when irradiated by 20, 200 and 800 MeV/u (MeV per atomic mass unit) proton, ^{3}He and ^{48}Ca ions using the PHITS and SRIM codes [4].

Figure 1 shows the depth dependence of the DPA per beam fluence for 5 cm radius and 0.1 cm thick copper and tungsten targets irradiated by 20 MeV/u beams. The DPA value in a material is related to the energy deposition. The ion ranges of proton, ^{3}He and ^{48}Ca are less than the mean free path for nuclear collisions with nuclear reactions, and therefore most of the ions stop without undergoing collisions. The energy dependence of the DPA value thus exhibits a so-called Bragg peak. Because the production rate of the

ISBN: 978-3-95450-202-8 doi:10.18429/JACoW-HB2018-TUP2WE03

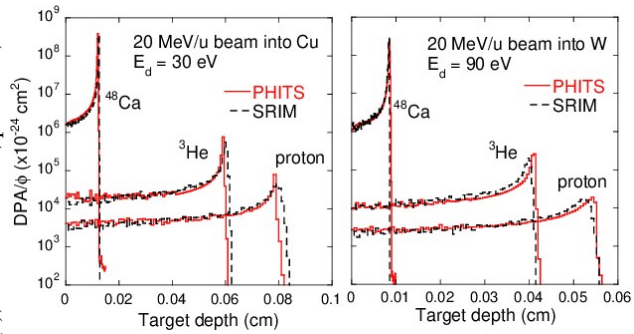

Figure 1: Depth dependence of DPA values per beam fluence for a 5 cm radius and 0.1 cm thick copper and 0.06 cm thick tungsten target irradiated by 20 MeV/u proton, ^{3}He and ^{48}Ca beams.

"secondary particles" is small, SRIM results are in good agreement with PHITS results .

In the cases of the 200 MeV/u proton and ^{3}He beams, nuclear collisions occur before the stopping range is reached, and displacement cross section contributions produced by PKA created by the "secondary particles" increase the overall DPA value at target depths smaller than the range, as shown by the PHITS results in Fig. 2. SRIM results however keep the shape of Bragg peak due to the lack of the nuclear reaction model.

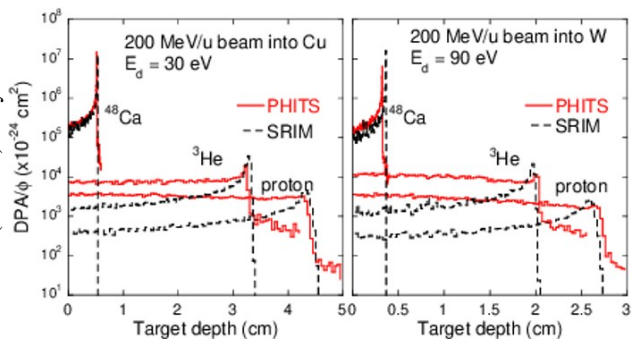

Figure 2: Depth dependence of DPA values per beam fluence for a 5 cm radius and 5 cm thick copper and 3 cm thick tungsten target irradiated by 200 MeV/u proton, ^{3}He and ^{48}Ca beams.

In the case of the 800 MeV/u proton and ^{3}He beams as shown in Fig. 3, the amount of production of the "secondary particle" is larger than that for the 200 MeV/u proton and ^{3}He beams, and the DPA values as a function of target depth shows the characteristics of well-developed hadronic cascade. Because many secondary protons are produced by nuclear reactions, a Bragg peak of the projectile is not appeared in Fig. 3. DPA values for the 800 MeV/u ^{48}Ca ion beam also exhibits an increase for target depths smaller than the ion beam range.

We can conclude that damage calculations using only PKA's directly created by the projectile, such as within SRIM, leads to severe underestimation when the projectile energy is high enough to create nuclear reactions. For

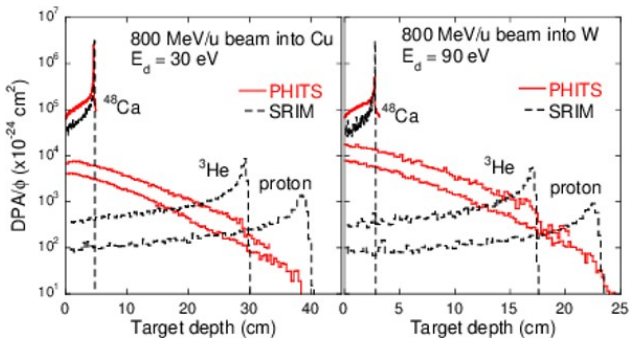

Figure 3: Depth dependence of DPA values per beam fluence for a 5 cm radius and 45 cm thick copper and 25 cm thick tungsten target irradiated by 800 MeV/u proton, ^{3}He and ^{48}Ca beams.

proton and ^{3}He beams, the DPA values near surface of the target increase with the incident energy (E>200 MeV/u) of ions [9].

BENCHMARKING EXPERIMENTS OF DISPLACEMENT CROSS SECTIONS

For validation of the displacement cross section calculations, we have obtained experimental displacement cross sections of copper in the case of 125, 200 MeV and 3 GeV proton irradiation using the Fixed-Field Alternating Gradient (FFAG) [17] accelerator facility at Institute for Integrated Radiation and Nuclear Science (KURNS) [11], the cyclotron facility at Research Center for Nuclear Physics (RCNP), Osaka University [12] and J-PARC [13, 14]. The experimental displacement cross section of aluminum was also obtained at RCNP. In this section, we introduce measurements of displacement cross sections of copper and aluminum under 200 MeV protons at RCNP.

Figure 4 shows a schematic of the cryogenic irradiation chamber with the GM cryocooler (RDK-408D2, Sumito-mo Heavy Industries, Ltd.) with a cooling capacity of 1 W at 4 K and the twin sample assembly connected to the 2nd stage of the cold head. The GM cryocooler cooled the sample by means of a conduction coolant via the aluminum plate and the oxigen-free high thermal conductivity copper (OFHC) block. The 1-mm-thick aluminum plates of the thermal radiation shield connected to the 40 K stage of the refrigerator covered the entire sample assembly to intercept any thermal radiation from the ambient irradiation chamber.

A pre-calibrated electrical resistance thermometer (Cernox thermometer, Lake Shore Cryotronics, Inc.) was attached in the OFHC block and the aluminum nitride (AlN) plate to confirm the cooling performance of the GM cryocooler. To simultaneously measure the changes in electrical resistivity of two samples under 200 MeV proton irradiation, two aluminum plates with the aluminum and copper wire samples were connected to the OFHC block by using bolts, as shown in Fig. 4.

Table 1 lists the characteristics of the wire samples. Each aluminum and copper wire with a 0.25-mm diameter, pur-

ISBN: 978-3-95450-202-8 doi:10.18429/JACoW-HB2018-TUP2WE03

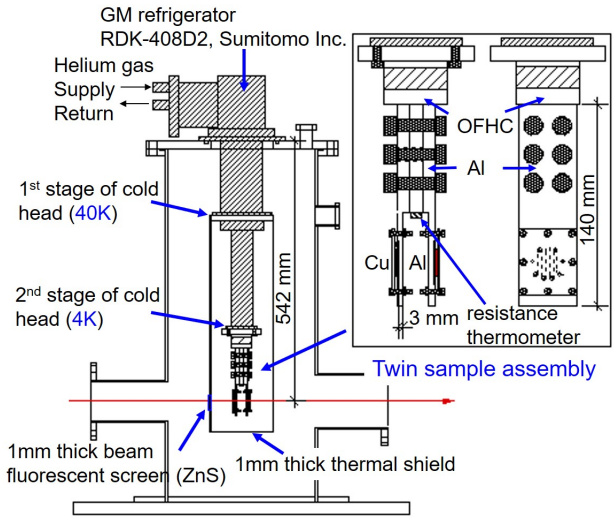

Figure 4: Schematic of cryogenic irradiation chamber and twin sample assembly with side view and view from beam upstream.

chased from the Nilaco Corporation, was set on the AlN plate in a serpentine-shaped line. The AlN plate was used because of its excellent electrical insulation and high thermal conductivity. Before irradiation, the aluminum wire and the copper wire were annealed in vacuum for 1 h at 550 °C (823 K) and 1100 °C (1273 K), respectively. The wire and the CX1050-SD Cernox resistance thermometer were carefully sandwiched between the 1-mm-thick AlN plate and the 1.5-mm-thick AlN plate.

Table 1: Characteristics of Wire Samples in the RCNP Experiment

Material	Aluminum	Copper
Diameter	0.25 mm	0.25 mm
Length	123 mm	134 mm
Electrical resistivity at room temperature	2.19×10^{-8} Ωm	1.47×10^{-8} Ωm
Electrical resistivity at 3 K	4.43×10^{-11} Ωm	2.02×10^{-11} Ωm

The electrical resistance of the wire was measured using an apparatus combining a current source (model 6221, Keithley Instruments, Inc.) and a nano-voltmeter (model 2182A, Keithley Instrument, Inc.). This apparatus is based on the current-reversal method (four-point technique) in the delta mode, which works by sourcing pulses with opposite polarity and taking one measurement during each pulse. A current of ±100 mA was fed into the copper wire with the polarity changing at a frequency of (10 Hz). The precision of this resistance measurement at 3 K was ±0.001 μΩ corresponding to an electrical resistivity of ±0.67 fΩm for aluminum and ±0.60 fΩm for copper, where the electrical resistivity of the sample ρ is expressed as follows:

$$\rho = RA/L \tag{12}$$

where R is the measured electrical resistance, L is the length between two potential points, and A is the area of the sample. The temperature of the Cernox resistance thermometer was measured using a temperature controller (model 335, Lake Shore Cryotronics, Inc.). According to the manual of the temperature controller, the accuracy of temperature measurement using the Cernox thermometer is 7.1 mK at 4.2 K.

The number of protons during irradiation was measured at the beam relative monitor in situ by counting the number of events produced by neutron-proton scattering at the 2.2 mg/cm^2 thick polyethylene in front of the cryogenic irradiation chamber [12]. Because the 200 MeV proton beam lost energy in the sample holder to materials such as AlN and aluminum plates in the beam line, the proton energies incident on the samples were estimated to be 185.3 ± 0.9 MeV for the aluminum wire and 195.5 ± 0.5 MeV for the copper wire, as determined using the PHITS code

The temperature increase due to beam heating was 1.2 K, 1.5 K, and 2.0 K in the cases of the 1.35 nA, 2.0 nA, and 3.0 nA currents, respectively, and the temperature was maintained below 5 K during beam irradiation. The electrical resistances of the aluminum and copper samples increased during beam irradiation owing to the production of defects in the wires. The total beam fluence on the sample was 3.89×10^{18} protons/m^2. The total increase in resistance was 0.76 μΩ for aluminum wire and 2.34 μΩ for copper wire. The damage rates of the aluminum and copper wires did not change considerably under proton irradiation with currents between 1.35 and 3.0 nA.

The displacement cross section can be related easily to the measured increase in resistivity and the calculated damage energy in the metal. The experimental displacement cross-section σ_{exp} was obtained using the measured damage rate, which is the ratio of the change in resistivity of metal $\Delta\rho_{metal}$ at around 5 K to the beam average fluence $\bar{\phi}$ [12]:

$$\sigma_{exp} = \Delta\rho_{metal}/(\rho_{FP}\cdot\bar{\phi}) \tag{13}$$

where ρ_{FP} is the change in resistivity per Frenkel-pair density for a particular metal (experimental data on ρ_{FP} were summarized and discussed in [18,19]). In this work, ρ_{FP} was set to 3.9 ±0.6 μΩm for aluminum [20] and 2.2 ± 0.5 μΩm for copper [21], and the same values were used for estimating the displacement cross section of the 125-MeV-proton-irradiation experiments [11], the 1.1- and 1.94-GeV-proton-irradiation experiments [22], the 3-GeV-proton-irradiation experiments [13, 14] and the Jung data [23] for the sake of comparison with our experimental data.

Figure 5 shows the experimental displacement cross-section data of aluminum and copper obtained in FFAG data [11], RCNP data [12], J-PARC data [13, 14], BNL data [22] and Jung data [23]. It is assumed that the increase in resistivity is the sum of resistivity-per-Frenkel-pair values.

ISBN: 978-3-95450-202-8 doi:10.18429/JACoW-HB2018-TUP2WE03

The displacement cross-sections with energies are almost constant with energies above 100 MeV.

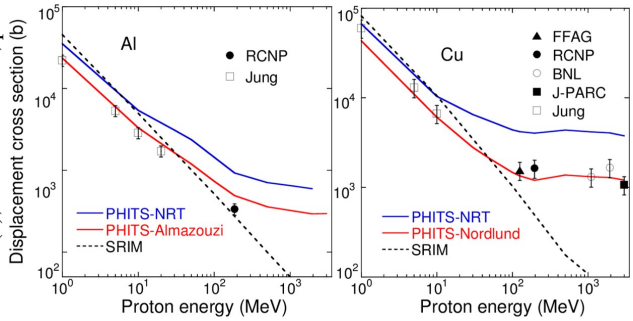

Figure 5: Displacement cross-sections for proton irradiation of aluminum (left) and copper (right): FFAG data [11] (black triangle), RCNP data [12] (black circles), BNL data [22] (open circles), J-PARC data [13, 14] (black square), Jung data [23] (open squares), NRT-dpa cross-section (blue line), the arc-dpa cross section (red line) and SRIM results (dashed line). The displacement energy is 27 eV for aluminum and 30 eV for copper.

Moreover, Fig. 5 shows results calculated by SRIM code, PHITS code with the NRT-dpa in Eq. (1) and the athermal-recombination-corrected displacement damage (arc-dpa) cross sections, which includes the results of the Molecular Dynamics simulation method (MD) for more accurate estimation of the actual damage production [24]. Because SRIM cannot calculate nuclear reactions, SRIM results are much smaller than others in high-energy region. The arc-dpa cross section was calculated using the efficiency function ζ [24].

$$\sigma_{arc-dpa} = \int_{t_d}^{t_{max}} d\sigma_{sc}/dt \cdot N_{NRT} \cdot \zeta \, dt \qquad (14)$$

$$\zeta = \frac{1 - c_{arc-dpa}}{(2E_d/0.8)^{b_{arc-dpa}}} T_d^{b_{arc-dpa}} + c_{arc-dpa} \qquad (15)$$

The arc-dpa displacement parameter is based on two tabulated parameters: $b_{arc-dpa}$, and $c_{arc-dpa}$. To obtain these parameters, the results of MD modelling were taken for aluminum from Almazouzi et al. [25] and copper from Nordlund et al. [24]. These parameters are listed in [12]. In terms of the cross sections of aluminum and copper in the experimental data and those determined using arc-dpa, PHITS with the efficiency function shows better agreement with the experimental data than with the NRT-dpa cross section, which has been widely used for radiation damage estimation. Further studies on measuring other metals under the low radiation damage are in progress, which will allow us to study the basic physics of point defects in the high-energy ion irradiation region.

CONCLUSION

The radiation damage calculation model in the PHITS cde has been developed to calculate the DPA value due to the target PKA created by the projectile and the secondary particles which include all particles created from the sequential nuclear reactions. For the DPA value in the high-energy (E>100 MeV) proton incident reactions, a target PKA created by the secondary particles was more dominant than a target PKA created by the projectile.

To validate predictions of displacement cross sections in copper and aluminum irradiated by >100 MeV protons, we developed a proton irradiation device with a GM cryocooler to cryogenically cool wire samples. By using this device, the defect-induced electrical resistivity changes related to the displacement cross section of copper were measured under irradiation with 125, 200 MeV and 3 GeV protons and that of aluminum under 200 MeV protons at cryogenic temperature. It is concluded that the experimental displacement cross sections agree better with calculated arc-dpa cross sections than with calculated NRT-dpa cross sections.

ACKNOWLEDGEMENTS

The authors wish to express their gratitude to Prof. Dr. M. Fukuda and the staff at RCNP for their generous support for beam operation. They also wish to thank to Prof. Dr. T. Ogitsu at KEK and the staff at KURNS, KEK and Japan Atomic Energy Agency (JAEA) for their generous support for device development. Y. Iwamoto wishes to express his gratitude to Prof. Dr. G. Bollen for his generous support to simulation study at MSU.

This work was supported by JSPS KAKENHI Grant Number JP16H04638. The calculation work was supported in part by the US National Science Foundation under grant PHY06-06007. The present study includes the results of "Measurement of displacement cross-section at J-PARC for structural material utilized at ADS" entrusted to JAEA by the Ministry of Education, Culture, Sports, Science and Technology of Japan (MEXT).

REFERENCES

[1] Facility for Rare Isotope Beams (FRIB), http://www.frib.msu.edu/

[2] Japan Proton Accelerator Research Complex (J-PARC), http://j-parc.jp/index-e.htm

[3] European Spallation Source (ESS), http://ess-scandinavia.eu/

[4] J. F. Ziegler, J. P. Biersack and U. Littmark, *The Stopping and Range of Ions in Solids*. New York, USA: Pergamon Press, 1985.

[5] T. Sato *et al.*, "Features of particle and heavy ion transport code system (PHITS) version 3.02", *J. Nucl. Sci. Technol.*, vol. 55, pp. 684–695, 2018, doi:10.1080/00223131.2017.1419890

[6] N.V. Mokhov *et al.*, "The MARS code system user's guide", Fermilab, Batavia, USA, Rep. Fermilab-FN-628, 1995.

[7] T. T. Bohlen *et al.*, "The FLUKA code: Developments and Challenges for High Energy and Medical Applications", *Nuclear Data Sheets*, vol. 120, pp. 211–214, 2014, doi:10.1016/j.nds.2014.07.049

ISBN: 978-3-95450-202-8 doi:10.18429/JACoW-HB2018-TUP2WE03

[8] L.S. Water *et al.*, "MCNPX user's manual version 2.4.0", Los Alamos National Laboratory, Los Alamos, New Mexico, USA, Rep. LA-CP-02-408, 2002.

[9] Y. Iwamoto *et al.*, "Improvement of radiation damage calculation in PHITS and tests for copper and tungsten irradiated with protons and heavy-ions over a wide energy range", *Nucl. Instr. Meth. B*, vol. 274, pp. 57–64, 2012, doi:10.1016/j.nimb.2011.11.038

[10] Y. Iwamoto *et al.*, "Calculation of displacement cross-sections for structural materials in accelerators using PHITS event generator and its applications to radiation damage", *J. Nucl. Sci. Technol.*, vol. 51, pp. 98–107, 2014, doi:10.1080/00223131.2013.851042

[11] Y. Iwamoto *et al.*, "Measurement of the displacement cross-section of copper ir-radiated with 125 MeV protons at 12 K", *J. Nucl. Mater.*, vol. 458, pp. 369–375, 2015, doi:10.1016/j.jnucmat.2014.12.125

[12] Y. Iwamoto *et al.*, "Measurement of displacement cross sections of aluminum and copper at 5 K by using 200 MeV protons", *J. Nucl. Mater.*, vol. 508, pp. 195–202, 2018, doi:10.1016/j.jnucmat.2018.05.038

[13] S. Meigo *et al.*, "Measurement of displacement cross-section for structural materials in high-power proton accelerator facility", presented at the 9th Int. Particle Accelerator Conf. (IPAC'18), Vancouver, Canada, Apr. 2018, paper MOPML045.

[14] S. Meigo *et al.*, "Beam instruments for high power spallation neutron source and facility for ADS in J-PARC", presented at the 61st ICFA Advanced Beam Dynamics Workshop on High-Intensity and High- Brightness Hadron Beams (HB2018), Daejeon, Korea, June 2018, paper TUP1WE03, this conference.

[15] G. S. Was, *Fundamentals of Radiation Materials Science, Materials and Alloys*. New York, USA: Springer Press, 2017.

[16] M. J. Norgett *et al.*, "A proposed method of calculating displacement dose rates", *Nucl. Engineering and Design*, vol. 33, pp. 50–54, 1975, doi:10.1016/0029-5493(75)90035-7

[17] S. L. Sheehy *et al.*, "Characterization techniques for fixed-field alternating gradient accelerators and beam studies using the KURRI 150 MeV proton FFAG", *Prog. Theor. Exp. Phys.*, 073G01(31 pages), 2016, doi:10.1093/ptep/ptw086

[18] A. Yu. Konobeyev *et al.*, "Evaluation of effective threshold displacement energies and other data required for the calculation of advanced atomic displacement cross-sections", *Nucl. Energy and Technology*, vol. 3, pp. 169–175, 2017, doi:10.1016/j.nucet.2017.08.007

[19] C. H. M. Broeders and A. Yu. Konobeyev, "Defect production efficiency in metals under neutron irradiation", *J. Nucl. Mater.*, vol. 328, pp. 197–214, 2004, doi:10.1016/j.jnucmat.2004.05.002

[20] P. Ehrhart and W. Schilling, "Investigation of interstitials in electron-irradiated aluminum by diffuse-X-Ray scattering experiments", *Phys. Rev. B*, vol. 8, pp. 2604–2621, 1973, doi:10.1103/PhysRevB.8.2604

[21] H. G. Haubold and D. Martinsen, "Structure determination of self-interstitials and investigation of vacancy clustering in copper by diffuse X-ray scattering", *J. Nucl. Mater*, vol. 69–70, pp. 644–649, 1978, doi:10.1016/0022-3115(78)90302-1

[22] G. A. Greene, "Direct measurements of displacement cross sections in cop-per and tungsten under irradiation by 1.1-GeV and 1.94-GeV protons at 4.7 K", in *Proc. 6th International Meeting on Nuclear Applications of Accelerator Technology (AccApp'03)*, San Diego, CA, USA, June 2004, pp. 881-892.

[23] P. Jung, "Atomic displacement functions of cubic metals", *J. Nucl. Mater*, vol. 117, pp. 70–77, 1983, 10.1016/0022-3115(83)90011-9

[24] K. Nordlund *et al.*, "Improving atomic displacement and replacement calculations with physically realistic damage models", *Nature Communications*, vol. 9, pp. 1084, 2018, doi:10.1038/s41467-018-03415-5

[25] A. Almazouzi *et al.*, "Defect production and damage evolution in Al: a molecular dynamics and Monte Carlo computer simulation", *Nucl. Instr. Meth. B*, vol. 153, pp. 105–115, 1999, doi:10.1016/S0168-583X(98)00989-6